ARTICLE

Organization of *Pseudomonas fluorescens* on Chemically Different Nano/Microstructured Surfaces

Carolina Díaz,[†] Roberto C. Salvarezza,[†] Mónica A. Fernández Lorenzo de Mele,[†,‡] and Patricia L. Schilardi*[,†]

Instituto de Investigaciones Fisicoquímicas Teóricas y Aplicadas (INIFTA), Facultad de Ciencias Exactas, Universidad Nacional de La Plata—CONICET, Casilla de Correo 16, Sucursal 4, (1900) La Plata, Argentina, and Facultad de Ingeniería, Universidad Nacional de La Plata, La Plata, Argentina

ABSTRACT This paper describes bacterial organization on nano/micropatterned surfaces with different chemical properties, which show different interactions with the biological systems (inert, biocompatible, and bactericide). These surfaces were prepared by molding techniques and exposed to *Pseudomonas fluorescens (P. fluorescens)* cultures. Results from atomic force microscopy and optical imaging demonstrate that the structure of *P. fluorescens* aggregates is strongly dependent on the surface topography while there is no clear linking with the physical-chemical surface properties (charge and contact angle) of the substrate immersed in abiotic culture media. We observe that regardless of the material when the surface pattern matches the bacterial size, bacterial assemblages involved in surface colonization are disorganized. The fact there is not a relationship between surface chemistry and bacterial organization can be explained by the coverage of the surfaces by adsorbed organic species coming from the culture medium. Viability assays indicate that copper behaves as a toxic substrate despite the presence of adsorbed molecules. The combination of surface traps and biocidal activity could act synergistically as a suitable strategy to limit bacterial spreading on implant materials.

KEYWORDS: biofilm • nanotopography • micropattern • copper • gold • cyanoacrylate

INTRODUCTION

In recent years, efforts have been made to improve the surface properties of implants in such a way that minimizes the reaction of the body to the foreign material, facilitating cell adhesion (i.e., osseointegration), and avoiding bacterial adhesion and motility on the surface (1). In this sense, strategies considering surface chemical modification (2) including self-assembled monolayers of molecules with different functional properties (3, 4), grafting (5), ion implant (6, 7), etc., and surface topographic modification by nano/microstructuring surfaces (8, 9) have been studied in order to control the interaction of the material with the biological medium.

Topographic effects on the adhesion and growth of eukaryote cells have already been reported (10—15). It was found that many types of cell were very sensitive even to small differences in the scale of the topography (16). Cells responded to topography although the most effective dimensions of the features vary from one cell type to another. However, the combined effects of topography and chemistry modification of solid surfaces on cell adhesion is still under debate (14).

One of the most common causes of implant failures is related to biofilm formation and subsequent infection. Although it is accepted that the surface roughness affects bacterial adhesion to implant surfaces, it was also proposed that the surface physical chemistry of the material has a strong impact in this process (17). In fact, the attachment of bacteria is not only influenced by topography but also by the hydrophobicity/hydrophilicity and surface charge of the substrate, and the bacterial surface charge, which is determined by ionic strength and pH. Even though plenteous information can be found in relation to the effects of surface properties on the adhesion of pioneer bacteria, i.e., bacteria that initiate the colonization of the surface, little is known about the impact of topography and physicochemical properties on the bacterial colonization rate, a key point related to implant infection. To study the fundamental aspects of bacterial organization, we need model surfaces, with different but controlled chemical and topographical properties.

Recently, we have demonstrated that engineering gold surfaces with patterns in the nano/micrometer range affects the structure of *Pseudomonas fluorescens (P. fluorescens)* aggregates related to adhesion and motility (18, 19). Patterns tuning bacterial diameter or motility elements disorganize bacterial aggregates, and induce changes in the direction, size, and shape of the cells.

The aim of this work is to study the combined effect of both topography and physicochemical properties of the substrate surface on *P. fluorescens* organization and to establish if one of them, topography or physicochemical properties, dominates the aggregation processes. These

* Corresponding author. Phone: 54 221 4257430/7291. Fax: 54 221 4254642. E-mail: pls@inifta.unlp.edu.ar; pls@quimica.unlp.edu.ar.
Received for review April 7, 2010 and accepted August 1, 2010
[†] Instituto de Investigaciones Fisicoquímicas Teoricas y Aplicadas (INIFTA), Facultad de Ciencias Exactas, Universidad Nacional de La Plata—CONICET.
[‡] Facultad de Ingeniería, Universidad Nacional de La Plata.
DOI: 10.1021/am100313z

Published on Web 08/20/2010

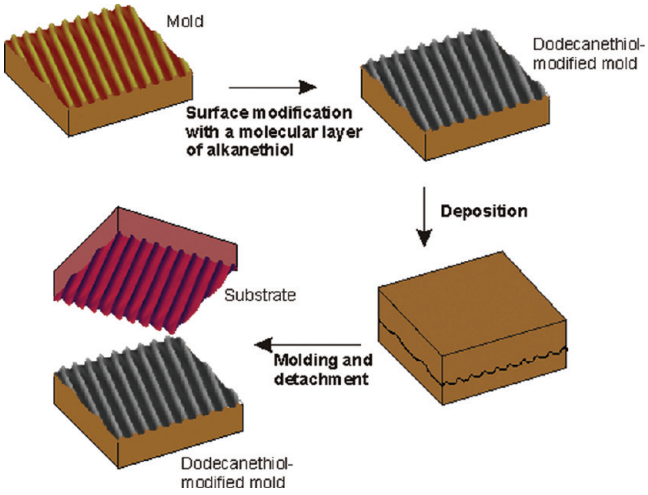

FIGURE 1. Schematic illustration of the complete procedure for fabrication of polymeric and metallic nano/microstructures by the nanotransfer molding method.

microorganisms are frequently used as model species for studying social motility of bacteria on solid surfaces. Accordingly, we have studied the initial stages of *P. fluorescens* organization on different nanostructured and submicrometer structured materials: gold (inert material), copper (biocidal material) and polyisobutylcyanoacrilate (PBCA), (highly biocompatible material). These substrates have different surface charge and hydrophilic/hydrophobic properties. We use atomic force microscopy and epifluorescence optical imaging to characterize bacteria organization on these substrates.

MATERIALS AND METHODS

Substrates. Microstructured (MS) patterned surfaces were prepared by molding and replication techniques, as described elsewhere (20, 21). Briefly, a copper mold surface was derivatized with a self-assembled dodecanethiol monolayer made by immersion in a dodecanethiol-containing toluene solution for 24 h, in order to avoid surface damages during the release step from the mold. The dodecanethiolate self-assembled monolayer (SAM) acts as an efficient antisticking layer covering the entire gold surface. The alkanethiolate-modified mold was then placed about 30 min in pure toluene to remove the physisorbed molecules forming multilayers. The deposition step comprised different procedures, according to the material-made film: (i) PBCA pouring directly on the mold surface; (ii) copper electrodeposition from 0.6 M $CuSO_4.5H_2O$ + 0.5 M H_2SO_4 + 0.024 mM thiourea electrolyte solution in a three-electrode conventional electrochemical cell (counterelectrode, copper foil; reference electrode, copper wire j = 20 mA cm^{-2}); (iii) thermal physical vapor deposition (PVD) of gold (operation pressure, 1 × 10^{-5} Pa, with the substrate kept at room temperature, resulting in a 200 nm thick gold layer). After PVD, a copper layer (about 10 μm thick) was electrodeposited (at the same conditions mentioned above) in the back of the film in order to have a mechanically stable gold substrate. The films were released from the mold using tweezers and immediately used as substrate. A scheme of the steps involved in surface molding is shown in Figure 1. As control, substrates of each material having randomly oriented grains of 50−100 nm in size have been used. Copper and gold controls are vapor deposited on random nanostructured metal (NS substrates) prepared by deposition of 200 nm metal layer on a glass covered by a thin Cr layer, purchased from Arrandee (Germany). The gold substrates were exposed for a while to butane flame, in order to eliminate any adsorbed environmental organic compounds, and then rinsed with Milli-Q water. With the purpose of emulate grains present on metallic surfaces, a PBCA NS substrate was prepared by molding techniques as described above by using a gold master with a hexagonal array of nanoholes (50 nm in size, 6 nm deep) covered by a dodecanethiol SAM. On this master, an aliquot of all-purpose commercial cyanoacrylate glue, used as alternative to suture for closing injuries (La Gotita, Poxipol, Argentina) was poured on the master and let it cure for 24 h. The PBCA layer was peeled off from the master, supported on a glass slide, and used as substrate for bacteria colonization. In the particular case of PBCA, we have also tested random "granular-like" microstructured surfaces (RMS) prepared by polymer casting on dodecanethiol-covered flame annealed vapor-deposited gold.

Bacterial Cultures and Adhesion. *P. fluorescens* were maintained in Cetrimide agar at 28 °C. The inoculum was prepared by suspending a Cetrimide agar slant (24 h old) in 2 mL of sterile nutrient medium. Afterward, the inoculum was poured into an Erlenmeyer flask containing 300 mL of the rich nutrient broth medium (Merck) and kept on a rotary shaker for 3 h at 28 °C. After 24 h growth, the substrates were placed into the culture for 2 h so as to allow bacterial adhesion. The substrates were then removed and washed gently by immersing in double distilled sterile water in order to eradicate those cells which were not tightly attached to the surface. Irreversibly adherent cells were fixed by drying in a nitrogen atmosphere at a relative humidity greater than 70%. A duplicate series of experiments and three numbers of replicates were carried out.

AFM and Epifluorescence Microscopy. Tapping and contact mode atomic force microscopy (AFM) (Nanoscope IIIa, Digital Instruments, Santa Barbara CA) was used to characterize the substrates using silicon tips (Nano World Arrow NCR, spring constant: 42 N/m, resonance frequency: 285 kHz) and silicon nitride tips (Veeco, Nanoprobes NP, spring constant: 0.12 N/m), respectively. Also, it was used to image early stages of biofilm formation at nanometer scale. In all cases, the topographic mode was used to image the samples.

To investigate the entire substrate colonization, we dyed cells with acridine orange and imaged by using epifluorescence miscroscopy technique. The samples were rinsed in double distilled sterile water and stained for 5 min with the fluorescent nucleic acid stain acridine orange at a concentration of 0.02% w/v. Next, samples were rinsed with double distilled sterile water to remove excess stain. Microbial cells attached to the substrate were imaged using an optical microscope (Olympus BX-51) with the WB 2# filter cube in the light path (excitation filter BP 450−480 nm).

Viability Assays. NS gold, NS copper, and NS PBCA substrates were each exposed to a *P. fluorescens* culture for 2 h. After that, the substrates were rinsed with NaCl solution 0.9 and dyed by using the LIVE/DEAD Baclight viability kit (Invitrogen). The Live/Dead kit includes the green fluorescent DNA-binding stain SYTO 9 and the red fluorescent DNA-binding stain propidium iodide (PI), enabling the determination of bacterial viability from the difference in membrane integrity in embedded cells. When used alone, the SYTO-9 stain generally labels all bacteria in a population, whereas propidium iodide penetrates only bacteria with damaged membranes, causing a reduction in the SYTO-9 stain. The live/dead stain was prepared by mixing 30 μL of staining component A (SYTO 9) and 30 μL of staining component B (propidium iodide) and diluting the mixture to 1/200 in distilled water. Six microliters of the dye was poured on each substrate and they were then kept in the dark for 15 min at room temperature. After that, the substrates were rinsed with sterile H_2O. Fluorescent bacteria were visualized by epifluorescence with an Olympus BX-51 microscope. The microscope filters used were U-MWG2 (excitation 510−550

nm and emission 590 nm) and U-MWB2 (excitation 460−490 and emission 520).

Bacterial viability was calculated from the ratio of the number of intact cells stained with SYTO-9 to the total number of cells (intact plus propidium iodine positive (damaged) cells). The measurements were made for at least 10 randomly recorded images.

Bacterial Surface Charge and Wetting Properties of the Substrate. The bacterial cell wall surface hydrophobicity and Lewis acid base electron donor/electron acceptor properties of the *P. fluorescens* were determined by MATS (Microbial Adhesion to Solvents) described by Bellon Fontaine et al. (22). This method is based on the comparison between microbial cell affinity to a monopolar solvent and an apolar solvent.

Equilibrium contact angle measurements have been carried out using a Ramé-Hart Model 500 goniometer (Ramé-Hart instrument Co., USA) in the contact angle mode with water as liquid probe. Each data of contact angle is the average result of 10 measurements performed on both, left and right side of the drop. Images were analyzed with DROPimage Advanced v2.2 software. In the case of copper, measurements after immersion of the substrate in the culture medium for 2 h were also made to assess the effect of organic substances adsorption on the wetting properties.

Electrochemical Measurements. To investigate surface charge and voltammetric response of the surface due to adsorbed species, open circuit potential and voltammetric runs were carried out using a three-electrode electrochemical cell. The potential was measured against a saturated calomel electrode (SCE) by using a potentiostat (PAR 362, EG&G Instruments). As counterelectrode, a platinum sheet was used. In the open circuit potential measurements, NS copper or NS gold substrates were used as working electrode and the *P. fluorescens* culture in nutrient broth was used as electrolyte. In the case of cyclic voltammetry, the working electrode was NS gold and the electrolyte was a 0.5% p/v NaCl solution. The substrate was immersed either in sterile broth or in serum albumin dissolution for different times and then used as working electrode in the electrochemical cell. To emulate the concentration of serum albumin contained in blood, 34 g/L dissolution was used. Serum albumin (Sigma-Aldrich, 99%) was dissolved as received in phosphate buffer solution (PBS) at pH 7.2.

RESULTS

For each material, gold, copper, and PBCA, two different types of patterned surfaces (NS, MS) were prepared. The AFM images of the NS gold (Figure 2a) and NS copper (Figure 2c) surfaces show small grains 75 ± 25 nm in size and 8 ± 2 nm in height (Figure 2a). The root-mean-square roughness (w) of these surfaces, defined as $\sqrt{\Sigma(z_i)^2/N}$ where z_i is the value of individual heights and N is the number of points, measured on 10 μm^2 AFM images is $w = 3$ nm and $w = 2.5$ nm for gold and copper, respectively. On the other hand, the AFM images of the PBCA surface (Figure 2e) reveal a hexagonal array of nanodots (10^{11} cm^{-2} dot density, 45 ± 5 nm in average size, 6 ± 1 nm in average height) with w = 5 nm, also measured on 10 μm^2 images. This PBCA surface was used to emulate the topography of "nanocrystalline" (NS) metal surfaces.

The second type of substrate, for gold, copper, and PBCA has a submicrostructured (MS) topography consisting in a grid of about 550 nm wide rows separated by 650 nm wide and average 120 nm deep channels for gold and PBCA (Figure. 2b,f) and 840 nm wide rows and 320 wide channels for copper, which implies that the wavelength and amplitude

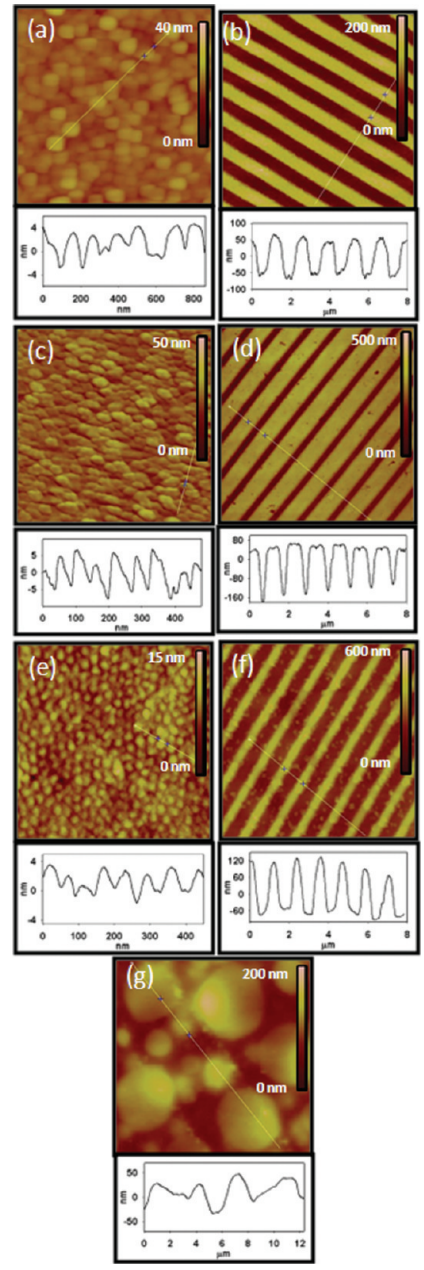

FIGURE 2. AFM images showing the typical features of the different nano/microstructured substrates used for bacteria colonization. The respective cross-section of each image is placed on bottom. (a) AFM image (topographic contact mode), 1 × 1 μm^2) of gold NS surface, (b) AFM image (topographic contact mode, 10 × 10 μm^2) of gold MS surface, (c) AFM image (topographic contact mode, 1 × 1 μm^2) of copper NS surface, (d) AFM image (topographic contact mode, 10 × 10 μm^2) of copper MS surface, (e) AFM image (topographic tapping mode, 1 × 1 μm^2) of a PBCA NS surface, (f) AFM image (topographic contact mode, 10 × 10 μm^2) of a PBCA MS surface; (g) AFM image (topographic tapping mode, 10 × 10 μm^2) of a RMS PBCA surface.

are 1.2 μm and 120 nm, regardless of the material. In this case the w value (from 10 μm^2 AFM images) is 39 nm.

The width of the channels tune very well with the bacterial diameter. Similar patterned features on gold surfaces have proved to show strong effects on the early stages of bacterial colonization, as previously reported (14). In the particular case of PBCA, we have also tested random "granular-like" microstructured surface (RMS) with grain size 1−5 μm, height 80−125 nm, and $w = 18$ nm (Figure 2g).

Table 1. Comparison of Topographic and Physicochemical Properties of the Different Substrates and Main Organization Structure of *P. fluorescens*[*]

	topographic properties			physicochemical properties			
substrate	pattern	wavelength (nm)	w (nm)	surface charge (mV), pH 7.7	contact angle	main organization structure	
gold	random nanocrystalline (NS)	75	3	pzc ≈ −600 mV (vs SCE)[c]	51.7 ± 0.1	raft + two-dimen-sional ordered aggregates	inert
	channels (MS)	1300	40		97.5 ± 0.3	isolated bacteria + disorganized rafts	
PBCA	nanodots (NS)	50	5	−30 near neutral[b]	83.7 ± 0.1	raft	biocompatible
	random granular (RMS)	2700	18		82.8 ± 0.2	disorganized rafts	
	channels (MS)	1300	40		78.1 ± 0.1	isolated bacteria + disorganized rafts	
Cu/Cu_2O	random nanocrystalline (NS)	81	2.5	pzc ≈ −310 mV (vs SCE)[a] IP ≈ 9.5	90.1 ± 0.1	isolated bacteria + three-dimensional aggregates	toxic for microbes
	channels (MS)	1400	37.3		98.6 ± 0.1	isolated bacteria + disorganized rafts	

[a] From ref 36. [b] From refe 37. [c] From ref 38. * Bacterial structures formed after immersion in the *P. fluorescence* culture for 2 h.

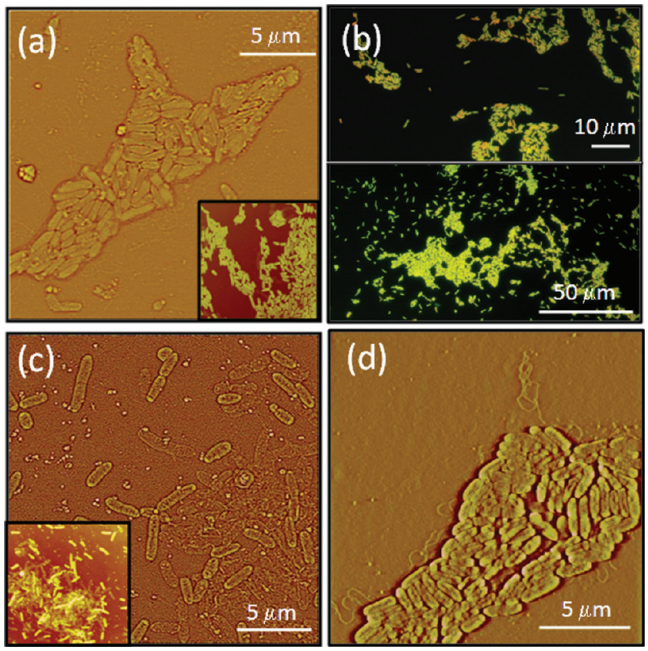

FIGURE 3. Images of *P. fluorescens* on NS substrates after 2 h of immersion in the *P. fluorescens* culture: (a) Gold (AFM, topographic contact mode, high pass filtered, 20.5 × 20.5 μm^2); inset: as-taken AFM image (topographic contact mode 19.7 × 19.7 μm^2) of bidimensional ordered aggregates. (b) Gold (epifluorescence image in liquid medium, for experimental details see the Supporting Information). (c) Copper (AFM, topographic contact mode, high pass filtered, 20.7 × 20.7 μm^2); inset: cumulus (AFM, topographic contact mode 20.6 × 20.6 μm^2). (d) PBCA (AFM, topographic contact mode, high pass filtered 17 × 17 μm^2). Flagella around aggregates can be clearly seen.

The surfaces described above were used to study bacterial colonization. The surface physical-chemical properties of the substrates are summarized in Table 1.

Bacterial Colonization on Nanostructured Surfaces (NS). Figure 3 shows AFM images of bacteria attached to the NS surfaces after 2 h of colonization. It should be noted that the resulting biofilm is formed by both, bacteria from broth and bacteria from duplication of the cells attached to the substrate.

On PBCA, the number of isolated bacteria on this surface is small. Most of the bacteria form close-packed aggregates where they are aligned forming raftlike structures (Figure 3d). Flagella can be clearly observed around the aggregates of cells. It has been reported that two-dimensional (2D) raftlike structures favors the displacement of moving bacteria across surfaces in a cooperative way, probably reducing the shielding stress with the liquid medium and the friction with the substratum with respect to those of isolated cell (19, 23, 24). This type of 2D aggregates can also be observed on NS gold surfaces (Figure 3a,b). Similarly to NS PBCA results, only a few isolated bacteria are detected. The identical bacterial behavior can be related to the nanostructure analogy of the substrates. Nanocrystalline gold have grains 75 nm in average size, matching the 50 nm dots in the polymer surface, and $w = 3$ nm, very close to the 5 nm measured for the polymer surface. Experiments made under 70% humidity (Figure 3a) and those in liquid media (Figure 3b) show identical results. On copper surfaces, we also observe isolated bacteria (Figure 3c) surrounding three-dimensional aggregates (inset in Figure 3c). In contrast to gold and PBCA, in this case the initial colonization proceeds by bacterial accumulation in a three-dimensional (3D) structure. A detailed inspection on large substrate areas shows no evidence of raftlike structures, as the aggregates are highly disorganized.

In order to explore the distribution and biological activity of cells on large areas of substrates, epifluorescence microscopy images were taken (Figure. 4). Bacteria shown in Figure 4 were dyed with acridine orange and imaged by epifluorescence microscopy. This dye is a nucleic-acid-selective fluorescent cationic dye useful for cell cycle determination. Acridine orange fluoresces either green or red, depending on the nature of the binding reaction with nucleic acid. The color of acridine orange-stained bacteria is frequently used as an indication of the activity of the cells. Actively metabolizing cells would be expected to have higher RNA content and thus appear orange with acridine orange staining (25). The three-dimensional structure of copper aggregates can

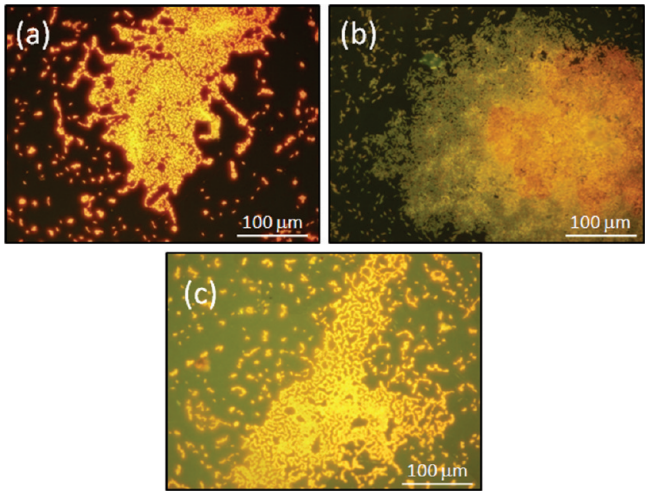

FIGURE 4. Epifluorescence microscopy images of NS substrate after 2 h of exposure to broth. (a) gold substrate; (b) copper substrate; (c) PBCA substrate.

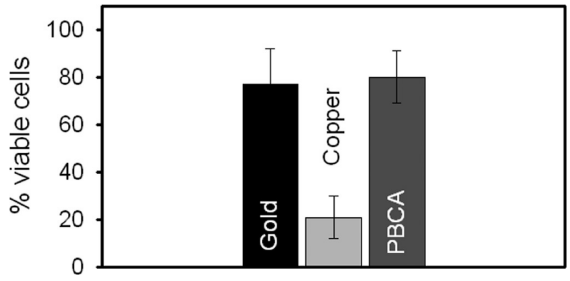

FIGURE 5. Percent of viable cells attached on gold, copper, and PBCA substrates.

be clearly seen in Figure 4b. A large amount of bacteria arranged in a rather disordered way forms the first layer of cells. Cells attached directly on the surface are green-colored, whereas those placed onto this first layer of bacteria fluoresce orange. These facts indicate a decrease in RNA production in the case of cells in contact with the toxic copper surface (26). On the other hand, bacteria forming the biofilm on gold and PBCA (Figure 4a, c) evidence a higher cell activity, indicated by orange florescence due to higher RNA production. In this context, it is valid to assume that on copper substrates, bacteria attached directly on the surface have a less cell activity, due to the toxic effect of copper ions and copper oxide on microbes. These qualitative results were quantified by viability assays carried out by using the Live/Dead BacLight kit. As can be seen in Figure 5, the number of viable cells attached on Au and PBCA substrates are markedly higher than those attached on copper surfaces.

Bacterial Colonization on Microstructured Surfaces (MS). It has been previously reported that the formation of raftlike structures are important in cooperative movement of bacteria colonizing a solid surface (23, 24). In particular, when swarming motility is involved, a certain level of wetness is required for movement (24). We have reported in previous works (18, 19) that MS topographies are good places for avoiding the formation of that raft-like structures and RMS surface features seem to fulfill the same role, as will be described in the next paragraphs.

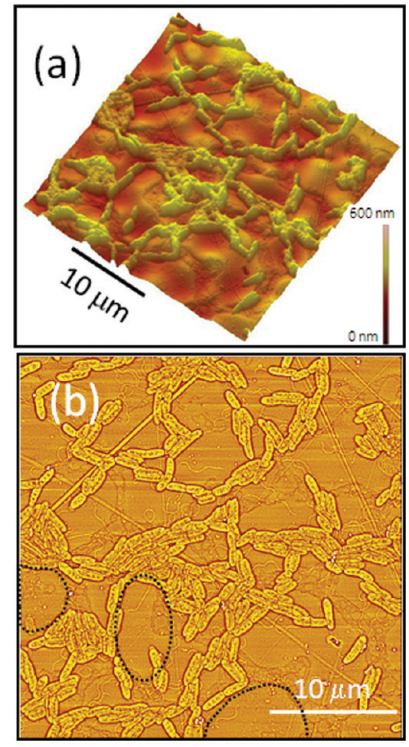

FIGURE 6. (a) 60 × 60 μm^2 AFM image, contact mode, of *P. fluorescens* on polymeric RMS substrates. (b) High pass filtered image of image a. Some granules are marked with dotted lines (see also Figure 2 g).

AFM images taken on a RMS polymer surface (Figure 2g) show that attached bacteria form randomly distributed long, open and ramified patterns formed by 1−5 bacteria in width (Figure 6a). Most of them are placed within the valleys around the polymer granules (Figure 6b). A close inspection of the ramified structures (Figure 6b) reveals that they are formed by aggregates of close packed and aligned bacteria, but they cannot reach the raftlike configuration. Flagella emerging from the cells are also clearly visible on the images and seem to connect neighboring cells. These images suggest that the random substrate microstructure hinder the formation of larger and well-organized rafts as those formed on the NS surfaces.

Interestingly, the organization of bacteria attached to MS surfaces is quite different to those formed on NS surfaces, irrespective of the substrate (Figure 7). In fact, we observed a large number of isolated bacteria trapped at the channels (see white arrows in Figure 7) aligned with the channel axis following the pattern direction. The other ones have preferred orientations that are mainly aligned forming 90−45° to the channels (Figure 7a,d). Epifluorescence images taken in liquid without drying the sample (Figure 7b) show that bacteria are aligned along the trenches that in this microscopy appear as bright stripes. More important, the aggregates formed on MS are smaller and more disorganized than the raftlike structures formed on NS. The possible sliding movements of the aggregates on the substrate seem to be hindered. In fact, only a few bacteria into the aggregates are aligned and close packed (Figure 7). In most cases, these aggregates appear oblique to the channels in such a way that avoid being trapped. It should be noted that

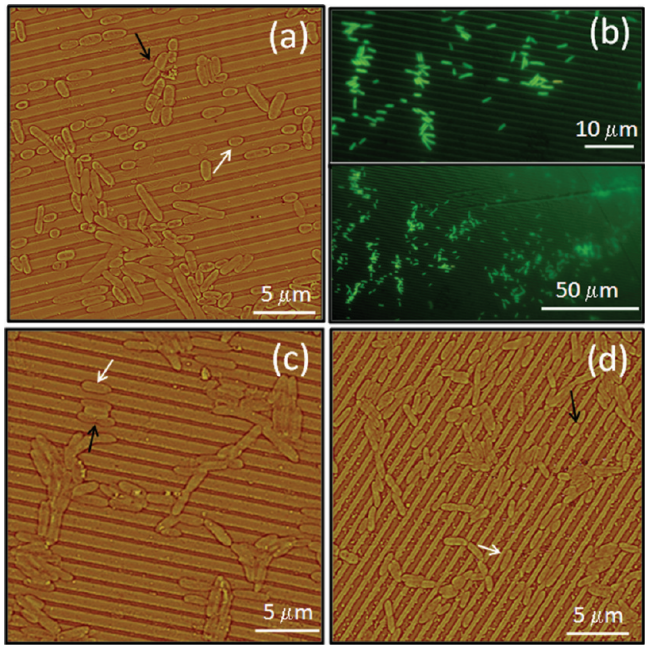

FIGURE 7. Images of *P. fluorescens* on MS substrates: (a) Gold (AFM, topographic contact mode, high pass filtered, 25 × 25 μm^2). (b) Gold (epifluorescence image in liquid medium, for experimental details see the Supporting Information). (c) Copper (AFM, topographic contact mode, high pass filtered, 24.3 × 24.3 μm^2). (d) PBCA (AFM, topographic contact mode, high pass filtered, 25 × 25 μm^2). White arrows show isolated bacteria; black arrows show apparently duplicated cells.

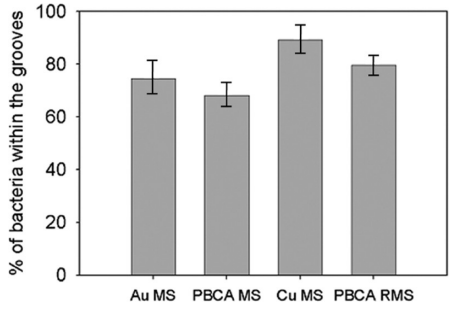

FIGURE 8. Statistical analysis of isolated bacteria placed within the grooves on MS and RMS surfaces.

if we only consider the isolated cells, those placed within the channels represent more than 70% of the cells in both, MS and RMS surfaces (Figure 8). The number of cells placed within the channels was calculated from the AFM images by counting them. This number was estimated from 10 different images. In the RMS case, this percentage is slightly larger than in the former, because those grooves are wider than cell size and thus more bacteria can be accommodated within the channels and reproduce within them.

It is worthwhile to compare the influence of the PBCA topography (roughness, wavelength) on bacterial organization. The average roughness and wavelength of the RMS are 18 nm and 2.7 μm, respectively, whereas the values for PBCA MS substrates are 40 nm and 1.3 μm, respectively (Table 1). This means that RMS substrates are smoother than MS surfaces, and with channel dimensions larger than bacteria size (Figure 6). In both cases, the whole effect is to hinder the formation of raftlike structures on RMS substrates, but the trapping of cells is less efficient than that on the MS

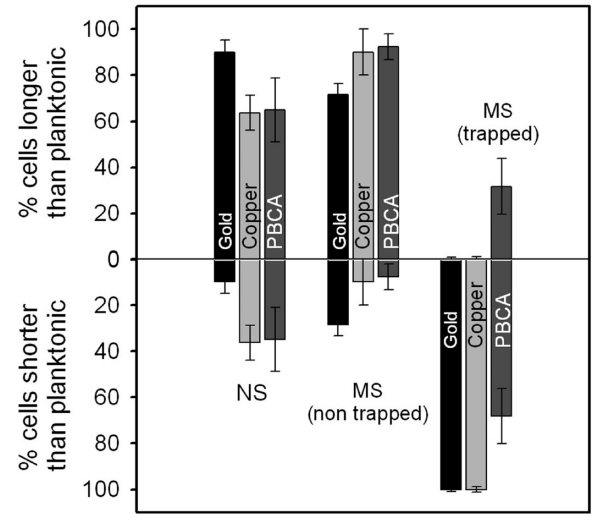

FIGURE 9. Histogram showing the percentage of bacteria attached on the different substrates that are longer or shorter than planktonic ones, represented as 0 line.

surfaces, where the size of channels matches the size of bacteria. However, bacteria seem to climb the channel wall easier than the RMS grains.

It has been reported that cells change their morphology in order to adapt to external conditions and to optimize mechanisms such as attachment to surfaces and motility (27). Also, changes in the morphology of cells depending on the characteristics of the substrate have been found (28). To compare the length of attached and planktonic cells, we measured the length of planktonic ones, resulting in 1.86 ± 0.6 μm, in good agreement with data reported in the literature (29). Statistical analysis of the attached bacterial length reveals different average values when it is compared with those obtained for planktonic cells. In fact, most bacteria attached on NS, in particular on gold, and nontrapped bacteria on MS substrates are longer than the average length of planktonic cells (Figure 9). In contrast, most of the trapped bacteria on gold, PBCA, and copper MS surfaces are shorter than the planktonic ones.

We speculate that this increase in length is due to the ability of nontrapped bacteria to move and colonize the surface by using swarming mechanism of motility as well as to connect neighboring aggregates. In fact, it has been reported that "swarm cells" are longer than single cells because elongation is favored by the alignment of the group by means of extensive side-by-side cell-to-cell contacts (27). This kind of alignment can be seen in Figure 3(a) and 3(d). In contrast, trapped bacteria on MS substrates cannot form rafts in order to move on the surface and in consequence they are shorter than those "free to move".

Surface Charge of *P. fluorescens*. The surface charge of *P. fluorescens* should be important in determining its interaction with substrate surfaces. Our results using MATS (22) indicate a higher affinity of the bacteria to chloroform, an acidic solvent, than hexadecane. The electron-donor character can be attributed to the presence of basic groups in the cell surface (22, 30) such as carboxyl (COO^-),

phosphate (PO_4^{2-}), and amino groups (NH_2). These results for *P. fluorescens* cells are in accordance with previous studies showing that *P. fluorescens* exhibits a negative zeta potential of −10 mV (31−33). Therefore, we can conclude that the bacteria exhibit a hydrophilic and negatively charged surface. This could explain why *P. fluorescens* seems to interact with positively charged polycrystalline gold surfaces displacing water and anions from the interface when they are immersed in a medium free of organic substances that can be adsorbed on the surface, as revealed by the increase in intensity with time of amide I and amide II protein bands in IR spectra (34).

DISCUSSION

There is plentiful information concerning the influence of the physicochemical properties of the substrate and bacterial surface (2−4), the medium properties (composition, ionic strength, pH, etc.) (35), and substrate topography (8, 9) on the initial attachment of individual cells. Subsequently to this attachment colonization proceeds and bacteria either join themselves to form a 3D structure or move and spread on the bare surface. In the present work, we study the effect of bacteria and substrates surface properties on bacterial organization for a particular medium composition and bacteria strain. Therefore, our results using three different materials with controlled topographies but markedly different physicochemical properties allow us to discuss the relative contribution of these factors on the organization of these bacteria.

Potential of zero charge (pzc), isoelectric point (IP), surface charge, and equilibrium contact angle data for our nano/microstructured surfaces are shown in Table 1. As expected, this data reveal that nanostructured gold is the only hydrophilic surface that turns hydrophobic when the surface patterns are introduced. PBCA and copper behave as hydrophobic surfaces irrespective of the topography.

Now we turn on the surface charge of our substrates. Electrochemical measurements show that the open circuit potentials value after 2 h of immersion in the culture media are 153 mV and −28 mV vs SCE for gold and copper, respectively. For gold the 153 mV value is more positive than the zero charge potential (Table 1) so that the gold surface is positively charged. The −28 mV value for the copper substrates is also more positive that the pzc of copper (−310 mV). However, electrochemical data indicate that in neutral media the copper surface is progressively covered by Cu_2O (39) so that the isoelectric point is a better variable to analyze surface charge. As copper exhibits IP ≈ 9.5 (Table 1) the surface charge of the copper substrate is also positive at the pH value of the culture media (pH 7.6). Finally, the PBCA surface is slightly negatively charged (Table 1). All these considerations are valid regardless of the substrate topography.

We start our discussion of the influence of physical chemical properties of the surface on bacterial organization on the nanostructured substrates on the light of the surface charge of the substrates and wettability. If surface charge is the main factor in cell organization, the positively charged gold and copper surfaces should promote similar bacterial

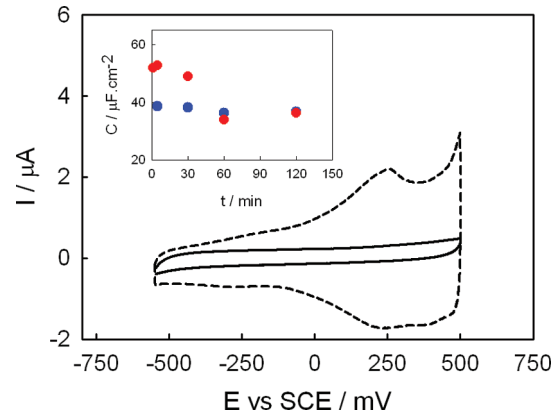

FIGURE 10. Cyclic voltammograms of gold in NaCl 0.5% p/v at 0.1 V/s. Dashed line, untreated gold; solid line, gold after 2 h of immersion in sterile broth. Inset, double layer capacitance vs time of immersion: red circles: gold immersed in sterile nutrient broth; blue circles: gold immersed in 34 g/L serum albumin dissolution.

adhesion and organization. However, the AFM and optical microscopy images reveal very different bacterial patterns. Notwithstanding that Au and PBCA have opposite surface charges they exhibit similar bacterial patterns. Therefore one can conclude that bacterial distribution and organization does not depend crucially on the surface charge that exhibit the bare substrate. The lack of correlation between surface charge and adhesion was also observed in previous studies (40). On the other hand, in these reports, the key role of hydrophobicity in promoting bacterial adhesion was emphasized (41). It has recently found that the hydrophilic *P. putida* adsorbs in an irreversible way on hydrophobic surfaces (dodecanethiol-covered gold) by dispersive forces while adsorption on hydrophilic surfaces (mercaptoundecanol-covered gold) is reversible (42). In the latter case, bacteria need to displace the water molecules from the surface turning this process unfavorable. A major role of hydrophobic groups, supposed to be associated with bacterial surface appendages, is suggested to be its dehydrating capacity, enabling the removal of the vicinal water film yielding small areas of direct contact between protuberant parts of the cell surface and the substratum (43, 44). In our case, Au is hydrophilic, whereas the Cu_2O covered surface is hydrophobic (45, 46), a difference that could explain the 2D to 3D dissimilar patterns. However, Au and PBCA exhibit similar 2D bacterial patterns being Au hydrophilic and PBCA closely hydrophobic (Table 1). Thus, although surface charge and wetting properties have been considered crucial factors in determining cell/surface interactions (47, 48) of pioneer bacteria, some recent works (49) and our results show no clear linking between these variables and bacterial adhesion.

We speculate that this behavior could be related to the presence of an adsorbed layer of organic substances from the culture media. To confirm the role of adsorbed organic matter present in the culture media in modifying the surface properties, we have performed different measurements. Figure 10 shows the voltammetric response in the double layer region of NS gold recorded in NaCl solution before and after 2 h of immersion in sterile broth. The capacitance of the electrochemical double layer is markedly reduced after

immersion in the sterile culture media. The inset shows the time dependence of the capacitance. It is evident that the gold surface is rapidly blocked due to the adsorption of organic species present in the culture media. A similar response has been observed for the adsorption of different negatively charged proteins on gold surfaces (34, 50). We have also measured the double layer capacitance of NS gold substrates in contact with an aqueous solution containing 34 g/L of serum albumin. Again our results show a marked decrease in the capacitance with the immersion time (Figure 10 inset), although the adsorption process is faster than that observed for the organic species present in broth. This observation is in agreement with previous results showing that the open circuit potential of gold in PBS reaches a constant value after 10−15 min of immersion in serum albumin (51). Note that the double layer capacitance of gold (Figure 10 inset) decreases after 2 h of immersion until reaching the same value, regardless of the solution.

The electrochemistry of oxide covered copper surfaces in chloride-containing media is much complex than that for gold, so that the behavior of the copper surfaces in contact with the sterile medium was explored using contact angle measurements. We observed that the angle of the water drop measured on NS copper surfaces changes from 90 to 66° after 2 h of immersion in sterile broth, indicating that the copper surface changes from hydrophobic to hydrophilic due to the adsorption of organic species coming from culture medium. It should be noted that although such adsorbed organic species change the wetting properties of the copper surface, they do not prevent the toxicity of the substrate, as the cellular activity of bacteria in contact with the surface remains lower than on Au after 2 h of exposure (Figures 4 and 5). From these results, it can be concluded that the properties of the substrate surfaces are rapidly modified by a hydrophilic layer of chemical species (mainly organic substances) coming from culture medium that change the surface properties of the bare material. We speculate that organic species (mainly proteins from the nutrient broth) displace adsorbed water molecules, as it is well-known that proteins adsorb on gold at open circuit potential. Moreover, after short periods of exposure, they block the surface hindering electron transfer processes (52). Thus, the surface modified by the hydrophilic layer seems to favor cell adhesion by specialized sites located on the flagella (42). Similar results have been found when SAMs- modified surfaces are incubated in fibrinogen dissolutions (53). Note that in some assays such as those reported in ref 35, bacteria are resuspended in a buffer solution and no organic matter from the culture media is present, in contrast to our system, where large amount of proteins is present. However, it should be noted that in real systems such as implantable materials, they are in direct contact with biological fluids that contain large amounts of proteins.

Another fact to be considered is that during the transition from reversible to irreversible adhesion on surfaces bacteria produce extracellular polymeric material (EPM), consisting of different molecules, ranging from homopolysaccharides to more complex heteropolysaccharides (54). Similar arguments to those mentioned previously have been used to interpret the difference of cell adhesion according to EPM production: If the amount of EPM is relatively small, cell adhesion onto solid surfaces is driven by electrostatic interaction, and if it is relatively large, cell adhesion is enhanced by polymeric interaction (55). Consequently, the presence of organic substances from the culture media or from EPM seems to have a similar influence in the sense of hindering the effect of electrostatic interactions, which consequently, do not have a key role in the organization of cells.

In contrast to chemical properties, a close inspection to Table 1 indicates that there is a good linking between bacterial organization and substrate topography. Smooth (nanocrystalline) gold and nanopatterned PBCA promote ordered aggregates and rafts, being the last the main structure found in PBCA. The formation of three-dimensional (3D) aggregates on copper rather two-dimensional (2D) structures can be explained considering copper ions toxicity that promotes bacterial gathering in such a way to exhibit the lowest number of cells in contact with the substrate. On the other hand, topography features tuning with bacterial diameter, results in the disorganization of the assemblage and then cooperative bacterial spreading could be restricted. The relationship between colonization and roughness is complex; however, our results show clearly that those surface features that act as "traps" hinder the formation of microbial structures related to the efficient collective bacterial motion on surfaces. This observation that was first reported on gold (18, 19) can be now extended to other kind of materials. Also noteworthy is the fact that the traps affect the formation of raftlike structures, but it does not seem to impede cell proliferation. Some evidence of bacterial duplication can be observed on the MS substrates (see arrows in Figure 7). It is possible that some of the dividing cells were not effectively adhered to the surface, but retained close to that by appendages or EPM material. In any case, daughter bacteria take part of cell aggregates because they could not be removed after rinsing.

The results presented in this work are in agreement with previous papers in which the adhesion and growth of eukaryotic cells was investigated from the point of view of chemical properties and surface topography (13−15, 56, 57). In those studies, results showed that the topography becomes more significant than chemistry of the surface for cell adhesion and orientation into grooves of different pitch when the depth of microfeatures were in the range of 0.5−1 μm[15]. It has been proposed that the response of the eukaryotic cells to topography involved the cytoskeleton of the cell to a marked extent (14). In our case, bacteria cells behave in a similar way, regardless of the chemical properties of surfaces when the depth of channels is at least 100 nm. On the other hand, we have previously reported that channeled nanostructured substrates of ∼40−250 nm wavelength and 4−20 nm in depth, have only small effects on bacterial adhesion and orientation (18).

Finally, a comment should be made on the experimental conditions used to image the bacteria organization on the different substrates. In fact, it could be hypothesized that the structure of the aggregates and bacterial shape and size are a consequence of capillary forces acting during sample drying (58). It is well-known that dewetting has strong influence on colloid distribution on surfaces (59−61). However, results recently reported indicate that adhesion of bacteria differ markedly from colloidal particles because of the presence of appendages that rearrange during the adhesion until bacteria are positioned in the energetically most favorable position (44). To eliminate this possibility we have made control experiments using the substrates kept immersed in sterile water. The results are shown in Figures 3b and 7b (see the Supporting Information for experimental details): the images taken with the immersed substrates exhibit the same morphologies as those imaged by AFM, i.e., bacterial rafts on NS substrates and isolated microbes trapped on MS substrates. This is not surprising because we are always working with a relative humidity larger than 70%, as it has been reported that a relative humidity of 55% allows maintenance of cell surface wettability and prevent cellular dehydration (62).

CONCLUSIONS

Results from atomic force microscopy and optical imaging demonstrate that the structure of bacterial aggregates formed during the early stage of biofilm formation in organic substances-containing media is strongly associated with the surface topography, roughness and toxicity, while there is no clear linking with the physicochemical surface properties (charge and contact angle). In fact, results show that cells respond in similar ways to the same topography on surfaces that are chemically very different. We assign the lost of chemical effects in our systems to the formation of a layer of adsorbed chemical species from broth and to the production of EPM by bacteria that change the original charge and wetting properties of the bare surface of the substratum. We observe that, irrespective of the material, only when the surface pattern tunes the microbial size, the organization of bacterial assemblage in rafts is hindered resulting in groups which are disorganized at the individual level. Viability assays indicate that copper behaves as a toxic substrate despite the presence of adsorbed organic molecules. Therefore, a reasonable speculation is that the suitable combination of surface traps on the substrate and a particular biocide could act synergistically as a proper strategy to limit bacterial spreading. This is a key point to reduce the rate of bacterial colonization of implantable materials.

Acknowledgment. The authors thank Agencia Nacional de Promoción Científica y Tecnológica (PICT 06-621, PICT 05-32906, PICT 33225, PAE 22771) UNLP, Project 11/X532 and 11/I129, and CONICET (PIP-6075) (Argentina). The authors also thank Dr. P. Peruzzo and J. Amalvy for contact angle measurements and Departamento de Sismologia e Informacion Meteorológica, Facultad de Ciencias Astronómicas y Geofísicas, UNLP, for relative humidity data.

Supporting Information Available: Experimental details concerning the assemblage of bacteria in liquid media (PDF). This material is available free of charge via the Internet at http://pubs.acs.org.

REFERENCES AND NOTES

(1) Subbiahdoss, G.; Grijpma, D. W.; Van Der Mei, H. C.; Busscher, H. J.; Kuijer, R. *J. Biomed. Mater. Res,. A* **2010**, *94* (2), 533–538.
(2) Araujo, E. A.; de Andrade, N. J.; da Silva, L. H. M.; de Carvalho, A. F.; de Silva, C. A. S.; Ramos, A. M. *Food Bioprocess Technol.* **2010**, *3* (3), 321–332.
(3) Burton, E. A.; Simon, K. A.; Hou, S.; Ren, D.; Luk, Y.-Y. *Langmuir* **2009**, *25* (3), 1547–1553.
(4) Hou, S.; Burton, E. A.; Simon, K. A.; Blodgett, D.; Luk, Y.-Y.; Ren, D. *Appl. Environ. Microbiol.* **2007**, *73* (13), 4300–4307.
(5) Shi, Z.; Neoh, K. G.; Kang, E. T. *Biomaterials* **2005**, *26* (5), 501–8.
(6) Yoshinari, M.; Oda, Y.; Inoue, T.; Shimono, M. *Metall. Mater. Trans., A* **2002**, *33* (3), 511–519.
(7) Xu, J.; Ding, G.; Li, J.; Yang, S.; Fang, B.; Sun, H.; Zhou, Y. *Appl. Surf. Sci.* **2010**; doi:10.1016/j.apsusc.2010.06.002.
(8) Weibel, D. B.; DiLuzio, W. R.; Whitesides, G. M. *Nat. Rev. Microbiol.* **2007**, *5* (3), 209–218.
(9) Ivanova, E. P.; Truong, V. K.; Wang, J. Y.; Berndt, C. C.; Jones, R. T.; Yusuf, I. I.; Peake, I.; Schmidt, H. W.; Fluke, C.; Barnes, D.; Crawford, R. J. *Langmuir* **2009**, *26* (3), 1973–1982.
(10) Karuri, N. W.; Liliensiek, S.; Teixeira, A. I.; Abrams, G.; Campbell, S.; Nealey, P. F.; Murphy, C. J. *J. Cell Sci.* **2004**, *117* (15), 3153–3164.
(11) Karuri, N. W.; Nealey, P. F.; Murphy, C. J.; Albrecht, R. M. *Scanning* **2008**, *30* (5), 405–413.
(12) Karuri, N. W.; Porri, T. J.; Albrecht, R. M.; Murphy, C. J.; Nealey, P. F. *IEEE Trans. Nanobiosci.* **2006**, *5* (4), 273–280.
(13) Curtis, A.; Wilkinson, C. *Mater. Today* **2001**, *4* (3), 22–28.
(14) Curtis, A. S. G. *Eur. Cell. Mater.* **2004**, *8*, 27–36.
(15) Britland, S.; Perridge, C.; Denyer, M.; Morgan, H.; Curtis, A.; Wilkinson, C. *Exp. Biol. Online* **1996**, *1* (2)), 1–15.
(16) Simon, K. A.; Burton, E. A.; Han, Y.; Li, J.; Huang, A.; Luk, Y.-Y. *J. Am. Chem. Soc.* **2007**, *129* (16), 4892–4893.
(17) An, Y. H.; Friedman, R. J., *Handbook of Bacterial Adhesion. Principles, Methods and Applications*; Springer: New York, 2000; p 672.
(18) Diaz, C.; Schilardi, P. L.; Salvarezza, R. C.; Fernandez Lorenzo de Mele, M. *Langmuir* **2007**, *23* (22), 11206–11210.
(19) Diaz, C.; Schilardi, P. L.; dos Santos Claro, P. C.; Salvarezza, R. C.; Fernandez Lorenzo de Mele, M. A. *ACS Appl. Mater. Interfaces* **2009**, *1* (1), 136–143.
(20) Azzaroni, O.; Fonticelli, M. H.; Benítez, G.; Schilardi, P. L.; Gago, R.; Caretti, I.; Vázquez, L.; Salvarezza, R. C. *Adv. Mater.* **2004**, *16* (5), 405–409.
(21) Azzaroni, O.; Schilardi, P. L.; Salvarezza, R. C. *Nano Lett.* **2001**, *1* (6), 291–294.
(22) Bellon-Fontaine, M. N.; Rault, J.; van Oss, C. J. *Colloids Surf., B* **1996**, *7* (1)), 47–53.
(23) Pelling, A. E.; Li, Y.; Cross, S. E.; Castaneda, S.; Shi, W.; Gimzewski, J. K. *Cell Motil. Cytoskeleton* **2006**, *63* (3), 141–148.
(24) Harshey, R. M. *Annu. Rev. Microbiol.* **2003**, *57* (1), 249–273.
(25) LV, E. *Biofilms: Recent Advances in Their Study and Control*; CRC Press: Boca Raton, FL, 2000; p 490.
(26) Borkow, G.; Gabbay, J. *Curr. Med. Chem.* **2005**, *12* (18)), 2163–2175.
(27) Young, K. D. *Curr. Opin. Microbiol.* **2007**, *10* (6), 596–600.
(28) Barton, L., *Structural and Functional Relationships in Prokaryotes*; Springer: New York, 2005; p xxvii.
(29) Ito, T.; Miyaji, T.; Nakagawa, T.; Tomizuka, N. *Biosci. Biotechnol. Biochem.* **2007**, *71* (2), 366–370.
(30) Briandet, R.; Meylheuc, T.; Maher, C.; Bellon-Fontaine, M. N. *Appl. Environ. Microbiol.* **1999**, *65* (12), 5328–5333.
(31) Smets, B. F.; Grasso, D.; Engwall, M. A.; Machinist, B. J. *Colloids Surf., B* **1999**, *14* (1)), 121–139.
(32) Valcarce, M. B.; Busalmen, J. P.; de Sanchez, S. R. *Int. Biodeterior. Biodegrad.* **2002**, *50* (1)), 61–66.
(33) Williams, V.; Fletcher, M. *Appl. Environ. Microbiol.* **1996**, *62* (1), 100–104.

(34) Busalmen, J. P.; Berna, A.; Feliu, J. M. *Langmuir* **2007**, *23* (11), 6459–6466.
(35) Sheng, X.; Ting, Y. P.; Pehkonen, S. O. *J. Colloid Interface Sci.* **2008**, *321* (2), 256–264.
(36) Lukomska, A.; Sobkowski, J. *J. Electroanal. Chem.* **2004**, *567* (1), 95–102.
(37) Kusonwiriyawong, C.; Lipipun, V.; Zhang, Q.; Ritthidej, G. C. *J. Controlled Release* **2008**, *132* (3), e6−e8.
(38) Yu, Y.; Jin, G. *J. Colloid Interface Sci.* **2003**, *268* (2), 288–292.
(39) Feng, Y.; Teo, W. K.; Siow, K. S.; Tan, K. l.; Hsieh, A. K. *Corros. Sci.* **1996**, *38* (3), 369–385.
(40) Teixeira, P.; Oliveira, R. *J. Adhes. Sci. Technol.* **1999**, *13* (11)), 1287–1294.
(41) Oliveira, R.; Azeredo, J.; Teixeira, P.; Fonseca, A. P. In *The Role Of Hydrophobicity In Bacterial Adhesion, Biofilm Community Interactions: Chance or Necessity?*; Contributions made at the Meeting of the Biofilm Club, 5, Powys, U.K., 2001; Gilbert, P. , Ed.; BioLine: Cardiff, U.K., 2001; pp11−22.
(42) Power, L.; Itier, S.; Hawton, M.; Schraft, H. *Langmuir* **2007**, *23* (10), 5622–5629.
(43) Busscher, H. J.; Weerkamp, A. H. *FEMS Microbiol. Lett.* **1987**, *46* (2), 165–173.
(44) Olsson, A. L. J.; van der Mei, H. C.; Busscher, H. J.; Sharma, P. K. *Langmuir* **2010**, *26* (13), 11113–11117.
(45) Mumm, F.; van Helvoort, A. T. J.; Sikorski, P. *ACS Nano* **2009**, *3* (9), 2647–2652.
(46) Ogwu, A. A.; Bouquerel, E.; Placido, F. *Coat. Mater. News* **2003**, *13* (4), n/a.
(47) Busalmen, J. P.; de Sanchez, S. R. *Appl. Environm. Microbiol.* **2001**, *67* (7), 3188–3194.
(48) Sheng, X.; Ting, Y. P.; Pehkonen, S. O. *J. Colloid Interface Sci.* **2007**, *310* (2), 661–669.
(49) Li, B.; Logan, B. E. *Colloids. Surf., B* **2004**, *36* (2), 81–90.
(50) Moulton, S. E.; Barisci, J. N.; Bath, A.; Stella, R.; Wallace, G. G. *Electrochim. Acta* **2004**, *49* (24), 4223–4230.
(51) Ying, P.; Viana, A. S.; Abrantes, L. M.; Jin, G. *J. Colloid Interface Sci.* **2004**, *279* (1), 95–99.
(52) Moulton, S. E.; Barisci, J. N.; Bath, A.; Stella, R.; Wallace, G. G. *J. Colloid Interface Sci.* **2003**, *261* (2), 312–319.
(53) Tegoulia, V. A.; Cooper, S. L. *Colloids Surf., B* **2002**, *24* (3−4), 217–228.
(54) Melo, L. F.; Bott, T. R.; Bernardo, C. A., *Fouling Science and Technology*; Kluwer Academic Publishers: Alvor, Portugal, 1987; Vol. 145.
(55) Tsuneda, S.; Aikawa, H.; Hayashi, H.; Yuasa, A.; Hirata, A. *FEMS Microbiol. Lett.* **2003**, *223* (2), 287–292.
(56) Curtis, A.; Wilkinson, C. *Biomaterials* **1997**, *18* (24), 1573–1583.
(57) Curtis, A. S. G.; Gadegaard, N.; Dalby, M. J.; Riehle, M. O.; Wilkinson, C. D. W.; Aitchison, G. *IEEE Trans. NanoBiosci.* **2004**, *3* (1), 61–65.
(58) Ploux, L.; Anselme, K.; Dirani, A.; Ponche, A.; Soppera, O.; Roucoules, V. *Langmuir* **2009**, *25* (14), 8161–8169.
(59) Celio, H.; Barton, E.; Stevenson, K. J. *Langmuir* **2006**, *22* (26), 11426–11435.
(60) Deegan, R. D.; Bakajin, O.; Dupont, T. F.; Huber, G.; Nagel, S. R.; Witten, T. A. *Phys. Rev. E* **2000**, *62* (1), 756.
(61) Tull, E. J.; Bartlett, P. N. *Colloids Surf., A* **2008**, *327* (1−3), 71–78.
(62) Mitik-Dineva, N.; Wang, J.; Truong, V. K.; Stoddart, P. R.; Malherbe, F.; Crawford, R. J.; Ivanova, E. P. *Biofouling* **2009**, *25* (7), 621–631.

AM100313Z